Spectroscopy of B_c mesons in the relativized quark model

Stephen Godfrey*

[1]*Ottawa-Carleton Institute for Physics, Department of Physics, Carleton University, Ottawa, Canada K1S 5B6*
[2]*Special Research Centre for the Subatomic Structure of Matter, University of Adelaide, Adelaide South Australia 5000, Australia*
(Received 28 June 2004; published 16 September 2004)

We calculate the spectrum of the charm-beauty mesons using the relativized quark model. Using the wave functions from this model we compute the radiative widths of excited $c\bar{b}$ states. The hadronic transition rates between $c\bar{b}$ states are estimated using the Kuang-Yan approach and are combined with the radiative widths to give estimates of the relative branching ratios. These results are combined with production rates at the Tevatron and the LHC to suggest promising signals for excited B_c states. Our results are compared with other models to gauge the reliability of the predictions and point out differences.

DOI: 10.1103/PhysRevD.70.054017 PACS numbers: 12.39.–x, 13.20.–v, 13.25.–k, 13.40.–f

I. INTRODUCTION

The charm-beauty (B_c) quarkonium states provide a unique window into heavy quark dynamics and therefore an important test of quantum chromodynamics. Although they are intermediate to the charmonium and bottomonium systems the properties of B_c mesons are a special case in quarkonium spectroscopy as they are the only quarkonia consisting of heavy quarks with different flavors. Because they carry flavor they cannot annihilate into gluons so are more stable with widths less than a hundred keV. Excited B_c states lying below BD (and BD^* or B^*D) threshold can only undergo radiative or hadronic transitions to the ground state B_c which then decays weakly. This results in a rich spectroscopy of narrow radial and orbital excitations below $B^{(*)}D^{(*)}$ threshold which are more stable than their charmonium and bottomonium analogues: There are two sets of S-wave states, as many as two P-wave multiplets (the $1P$ and some or all of the $2P$) and one D-wave multiplet below BD threshold. As well, the F-wave multiplet is sufficiently close to threshold that they may also be relatively narrow due to angular momentum barrier suppression of the Zweig allowed strong decays.

The discovery of the B_c meson by the Collider Detector at Fermilab (CDF) Collaboration [1] in $p\bar{p}$ collisions at $\sqrt{s} = 1.8$ TeV has demonstrated the possibility of the experimental study of this system and has stimulated considerable interest in B_c spectroscopy [2–14]. Calculations of B_c cross sections at hadron colliders predict that large samples of B_c states should be produced at the Tevatron and at the LHC opening up this new spectroscopy [15–25]. At the Tevatron it is estimated that $\mathcal{O}(10^7)B_c$ mesons should be produced for 1 fb^{-1} of integrated luminosity while at the LHC $\mathcal{O}(10^9)B_c$ mesons are expected to be produced for $L = 100$ fb^{-1}. These numbers are highly sensitive to the p_T and rapidity cuts used to extract the signal [17,18]. The B_c^* cross sections are expected to be $50 - 100\%$ larger than the B_c cross sections [16,19,20] and Cheung and Yuan [20,23] predict excited P-waves to contribute 20% of inclusive B_c production while D-wave states are expected to contribute about 2% [24]. Chang and Chen [22] and Cheung [19] estimate that the $2S$ states will be produced in roughly the ratio of $2S/1S \simeq 0.6$. It should therefore be possible to start exploring $c\bar{b}$ spectroscopy at the Tevatron, producing the $1P$ and $2S$ states and possibly even some $1D$ and $2P$ states with sufficient rate to be observed. At the LHC, with its higher luminosity, the D-wave $c\bar{b}$ states should be produced in a sizable number so that the LHC should allow the study of the spectroscopy and decay of B_c mesons.

In this paper we study the spectroscopy, including radiative transitions, of charm-beauty mesons using the relativized quark model [6,26,27]. The model includes one-gluon exchange with a running coupling constant and a linear confining potential. It uses relativistic kinematics and momentum dependent and nonlocal interactions. Although this model is not a rigorous calculation from first principles it gives a good account of most known mesons and baryons with only a few free parameters [6,26–29] so that it provides a useful guide to missing states. We compare its predictions to those of other models with the aim of highlighting which predictions are most sensitive to details of the models and therefore the most useful in distinguishing models. However, we are also interested in pointing out which predictions give the greatest agreement between models and therefore offer the most robust signatures for experiments to look for. Observation of these states and measurement of their properties would provide valuable information distinguishing details of the various models.

We start with a brief outline of the relativized quark model and comment on its similarities and differences with other quark model calculations. The spectroscopic predictions are given and compared to those of other models in the literature. This is followed by predictions for E1 and M1 radiative transitions and estimates of

*Email: godfrey@physics.carleton.ca

hadronic transitions based on the Kuang-Yan approach [30,31]. We summarize existing predictions for some of the more prominent weak decays of the B_c ground state as final states are an important ingredient in reconstructing the B_c mesons. In addition, leptonic decays measure the wave function at the origin and are therefore an additional test of the model [32]. We end by discussing some strategies for searching for excited B_c mesons and studying their spectroscopy.

II. SPECTROSCOPY

In this section we give the mass predictions of the relativized quark model [6,26,27] for the charm-beauty mesons and compare those predictions with the predictions of other calculations. This model has ingredients common to many quark potential models [4,8–10,12]. Almost all such models are based on some variant of the Coulomb plus linear potential expected from QCD. An interesting observation is that all recent models have arrived at the same slope for the linear confining potential of $\sim 0.18\ \mathrm{GeV}^2$. Most models, as does ours, also include the running constant of QCD, $\alpha_s(Q^2)$. And finally, relativistic effects are often included at some level. The relativized quark model has been reasonably successful in describing most known mesons. Although cracks have recently appeared with the discovery of the D_{sj} [33–35] and $X(3872)$ states [36], these point to the need to include physics which has hitherto been neglected such as coupled channel effects [37].

In the relativized quark model mesons are approximated by the $q\bar{q}$ sector of Fock space, in effect integrating out the degrees of freedom below some distance scale, μ^{-1}. This results in an effective potential, $V(\vec{p}, \vec{r})$, whose dynamics are governed by a Lorentz vector one-gluon-exchange interaction at short distance and a Lorentz scalar linear confining interaction. The basic equation of the model is the rest frame Schrödinger-type equation [38]:

$$H|\psi\rangle = [H_0 + V_{q\bar{q}}(\vec{p}, \vec{r})]|\psi\rangle = E|\psi\rangle \tag{1}$$

where

$$H_0 = \sqrt{p^2 + m_q^2} + \sqrt{p^2 + m_{\bar{q}}^2} \tag{2}$$

The effective quark-antiquark potential, $V_{q\bar{q}}(\vec{p}, \vec{r})$, was found by equating the scattering amplitude of free quarks, using a scattering kernel with the desired Dirac structure, with the effects between bound quarks inside a hadron [39,40]. Due to relativistic effects the potential is momentum dependent in addition to being coordinate dependent. To first order in $(v/c)^2$, $V_{q\bar{q}}(\vec{p}, \vec{r})$ reduces to the standard nonrelativistic result:

$$V_{q\bar{q}}(\vec{p}, \vec{r}) \to V(\vec{r}) = H_{q\bar{q}}^{conf} + H_{q\bar{q}}^{cont} + H_{q\bar{q}}^{ten} + H_{q\bar{q}}^{s.o.} \tag{3}$$

where

$$H_{q\bar{q}}^{conf} = C + br - \frac{4}{3}\frac{\alpha_s(r)}{r} \tag{4}$$

includes the spin-independent linear confinement and Coulomb-like interaction,

$$H_{q\bar{q}}^{cont} = \frac{32\pi}{9}\frac{\alpha_s(r)}{m_q m_{\bar{q}}}\vec{S}_q \cdot \vec{S}_{\bar{q}}\delta^3(\vec{r}) \tag{5}$$

is the color contact interaction,

$$H_{q\bar{q}}^{ten} = \frac{4}{3}\frac{\alpha_s(r)}{m_q m_{\bar{q}}}\frac{1}{r^3}\left[\frac{3\vec{S}_q \cdot \vec{r}\vec{S}_{\bar{q}} \cdot \vec{r}}{r^2} - \vec{S}_q \cdot \vec{S}_{\bar{q}}\right] \tag{6}$$

is the color tensor interaction,

$$H_{q\bar{q}}^{s.o.} = H_{q\bar{q}}^{s.o.(cm)} + H_{q\bar{q}}^{s.o.(tp)} \tag{7}$$

is the spin-orbit interaction with

$$H_{q\bar{q}}^{s.o.(cm)} = \frac{4\alpha_s(r)}{3r^3}\left(\frac{\vec{S}_q}{m_q m_{\bar{q}}} + \frac{\vec{S}_{\bar{q}}}{m_q m_{\bar{q}}} + \frac{\vec{S}_q}{m_q^2} + \frac{\vec{S}_{\bar{q}}}{m_{\bar{q}}^2}\right) \cdot \vec{L} \tag{8}$$

its color magnetic piece arising from one-gluon exchange and

$$H_{q\bar{q}}^{s.o.(tp)} = -\frac{1}{2r}\frac{\partial H_{q\bar{q}}^{conf}}{\partial r}\left(\frac{\vec{S}_q}{m_q^2} + \frac{\vec{S}_{\bar{q}}}{m_{\bar{q}}^2}\right) \cdot \vec{L} \tag{9}$$

the Thomas precession term. In these formulas $\alpha_s(r)$ is the running coupling constant of QCD.

To relativize the $q\bar{q}$ potential, the full Dirac scattering amplitude was used as a starting point which for on-shell $q\bar{q}$ scattering is exact. However for a strongly interacting system there will in general be off-shell behavior which we did not consider in addition to other simplifications such as neglecting more complex components of Fock space. We therefore built a semiquantitative model of relativistic effects by smearing the coordinate $\vec{r}$ over the distances of the order of the inverse quark mass by convoluting the potential with a Gaussian form factor and replacing factors of m_i^{-1} with, roughly speaking, factors of $(p^2 + m_i^2)^{-1/2}$. The details of this *relativization* procedure and the method of solution can be found in Ref. [6]. It should be kept in mind that because we neglected coupled channel effects and the crudeness of the relativization procedure we do not expect the mass predictions to be accurate to better than $\sim 10 - 20$ MeV.

For the case of a quark and antiquark of unequal mass charge conjugation parity is no longer a good quantum number so that states with different total spins but with the same total angular momentum, such as the $^3P_1 - {}^1P_1$ and $^3D_2 - {}^1D_2$ pairs, can mix via the spin-orbit interaction or some other mechanism. Eqs. (8) and (9) can be rewritten to explicitely give the antisymmetric spin-orbit mixing term:

$$H^{-}_{s.o.} = +\frac{1}{4}\left(\frac{4}{3}\frac{\alpha_s}{r^3} - \frac{b}{r}\right)\left(\frac{1}{m_Q^2} - \frac{1}{m_{\bar{Q}}^2}\right)\vec{S}_- \cdot \vec{L} \qquad (10)$$

where $\vec{S}_- = \vec{S}_Q - \vec{S}_{\bar{Q}}$. Consequently, the physical $j = 1$ P-wave states are linear combinations of $^3P_1$ and $^1P_1$ which we describe by:

$$P' = {}^1P_1 \cos\theta_{nP} + {}^3P_1 \sin\theta_{nP}$$
$$P = -{}^1P_1 \sin\theta_{nP} + {}^3P_1 \cos\theta_{nP} \qquad (11)$$

with analogous notation for the corresponding $L = D, F$, etc., pairs. In Eq. (11) $P \equiv L = 1$ designates the relative angular momentum of the $Q\bar{Q}$ pair and the subscript $J = 1$ is the total angular momentum of the $Q\bar{Q}$ pair which is equal to L. Our notation implicitely implies $L - S$ coupling between the quark spins and the relative orbital angular momentum. In the heavy quark limit in which the heavy quark mass $m_Q \to \infty$, the states can be described by the total angular momentum of the light quark, j, which couples to the spin of the heavy quark and corresponds to $j - j$ coupling. This limit gives rise to two doublets, one with $j = 1/2$ and the other with $j = 3/2$ and corresponds to two physically independent mixing angles $\theta = -\tan^{-1}(\sqrt{2}) \simeq -54.7°$ and $\theta = \tan^{-1}(1/\sqrt{2}) \simeq 35.3°$ [41]. Some authors prefer to use the $j - j$ basis [2] but since we solve our Hamiltonian equations assuming $L - S$ eigenstates and then include the LS mixing we use the notation of Eq. (11). It is straightforward to transform between the $L - S$ basis and the $j - j$ basis. It will turn out that radiative transitions are particularly sensitive to the $^3L_L - {}^1L_L$ mixing angle with predictions from different models in some cases giving radically different results. We also note that the definition of the mixing angles are fraught with ambiguities. For example, charge conjugating $c\bar{b}$ into $b\bar{c}$ flips the sign of the angle and the phase convention depends on the order of coupling $\vec{L}$, $\vec{S}_Q$ and $\vec{S}_{\bar{Q}}$ [41].

The Hamiltonian problem was solved using the following parameters: the slope of the linear confining potential is 0.18 GeV^2, $m_c = 1.628$ GeV, and $m_b = 4.977$ GeV. The predictions of our model are given in Fig. 1 and are compared to the predictions of other calculations in Table I. Because the mixing angles defined in Eq. (11) are important for predictions of radiative transitions those predictions are also given in Table I. Although I have attempted to consistently give the masses and the mixing angles of the predicted eigenstates in the convention of Eq. (11), because not all authors have unambiguously defined their phase conventions I cannot guaranty that these results are free of inconsistencies.

The different models are in remarkable agreement with the differences, for the most part, within the expected accuracy of the models. This almost certainly indicates how the various models have converged to using similar confining potentials and including a strong running coupling constant in the Coulomb piece of the potential. The only significant difference is the larger spread ($\sim$ 70 MeV) for the $1D$ multiplet center of gravity predictions. The spin-dependent splittings are also in reasonable agreement. Potential models can therefore be used as a reliable guide in searching for the B_c excited states. An important difference in the predictions is that in the Eichten-Quigg calculation [2] the $1P_1$ states are almost pure $^3P_1$ and $^1P_1$ with little mixing while in other models there is significant mixing. This arises from the much smaller expectation value of the off-diagonal mixing term [Eq. (10)] in the Eichten-Quigg calculation [2] compared to the other models. Since, after rotating from the $j - j$ basis to the $L - S$ basis, the $L - S$ mixing term given by Eichten and Quigg is in agreement with Eq. (10), the differences in expectation values can only be attributed to differences in the cancellations between the short and long distance pieces in Eq. (10), i.e., between the $\frac{4}{3}\frac{\alpha_s}{r^3}$ and $\frac{b}{r}$ pieces. This reflects subtle differences in the $q\bar{q}$ potentials of different models. Because the E1 radiative transitions are sensitive to the $^3P_1 - {}^1P_1$ mixing, the measurement of radiative transitions can be used to distinguish between the different models. The study of B_c spectroscopy will help test and refine the quark potential models but more importantly will test Lattice QCD, NRQCD, and pNRQCD, etc., which are more directly connected to QCD.

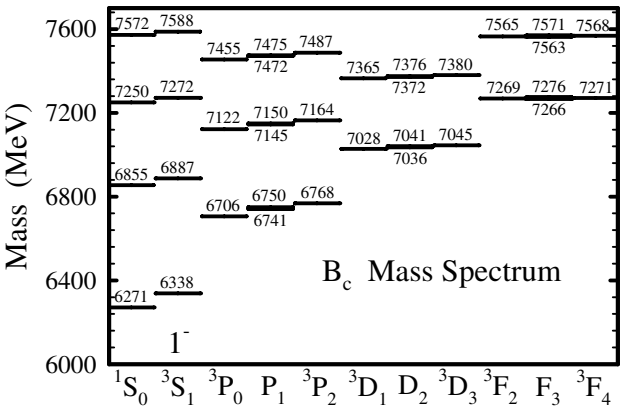

FIG. 1. The B_c mass spectrum.

III. RADIATIVE TRANSITIONS

Radiative transitions will likely play an important role in the discovery and identification of B_c states. In this section we calculate the E1 and M1 radiative widths. The partial width for an E1 radiative transition between states in the nonrelativistic quark model is given by [43]

$$\Gamma(\mathrm{n}^{2S+1}\mathrm{L}_J \to \mathrm{n}'^{2S'+1}\mathrm{L}'_{J'} + \gamma) = \frac{4}{3}\langle e_Q\rangle^2 \alpha\omega^3 C_{fi}\delta_{SS'}|\langle \mathrm{n}'^{2S'+1}\mathrm{L}'_{J'}|r|\mathrm{n}^{2S+1}\mathrm{L}_J\rangle|^2, \qquad (12)$$

TABLE I. Predicted masses and Spin-Orbit mixing angles. The first column labeled GI is the present work. The $P_1' - P_1$, $D_2' - D_2$, and $F_3' - F_3$ states and mixing angles are defined using the convention of Eq. . (11).

State	GI[6]	EFG [12]	FUII [10]	GKLT [5]	EQ [2]	GJ [9]	ZVR [8]	Lattice [42][a]
1^3S_1	6338	6332	6341	6317	6337	6308	6340	6321 ± 20
1^1S_0	6271	6270	6286	6253	6264	6247	6260	$6280 \pm 30 \pm 190$
1^3P_2	6768	6762	6772	6743	6747	6773	6760	6783 ± 30
$1P_1'$	6750	6749	6760	6729	6736	6757	6740	6765 ± 30
$1P_1$	6741	6734	6737	6717	6730	6738	6730	6743 ± 30
1^3P_0	6706	6699	6701	6683	6700	6689	6680	6727 ± 30
θ_{1P}	22.4°	20.4°	28.5°	17.1°	$\sim -2°$	25.6°		$33.4 \pm 1.5°$
2^3S_1	6887	6881	6914	6902	6899	6886	6900	6990 ± 80
2^1S_0	6855	6835	6882	6867	6856	6853	6850	6960 ± 80
2^3P_2	7164	7156		7134	7153		7160	
$2P_1'$	7150	7145		7124	7142		7150	
$2P_1$	7145	7126		7113	7135		7140	
2^3P_0	7122	7091		7088	7108		7100	
θ_{2P}	18.9°	23.2°		21.8°	−17°			
3^3S_1	7272	7235			7280		7280	
3^1S_0	7250	7193			7244		7240	
1^3D_3	7045	7081	7032	7007	7005		7040	
$1D_2'$	7036	7079	7028	7016	7009[b]		7030	
$1D_2$	7041	7077	7028	7001	7012[b]		7020	
1^3D_1	7028	7072	7019	7008	7012		7010	
θ_{1D}	44.5°	−35.9°		−34.5°				
1^3F_4	7271						7250	
$1F_3'$	7266						7250	
$1F_3$	7276						7240	
1^3F_2	7269						7240	
θ_{1F}	41.4°							

[a]The error estimates are taken from Ref. [10]
[b]We identify the $1D_2'$ and $1D_2$ states with the $^1D_2$ and $^3D_2$ states of Eichten and Quigg [2]

where

$$\langle e_Q \rangle = \frac{m_b e_c - m_c e_{\bar{b}}}{m_b + m_c} \tag{13}$$

$e_c = 2/3$ is the c-quark charge and $e_b = -1/3$ is the b-quark charge in units of $|e|$, α is the fine-structure constant, ω is the photon's energy, and C_{fi} is given by

$$C_{fi} = \max(L, L')(2J' + 1)\begin{Bmatrix} L' & J' & S \\ J & L & 1 \end{Bmatrix}^2. \tag{14}$$

For convenience the C_{fi} coefficients are listed in Table II and III. The matrix elements $\langle n'^{2S'+1}L'_{J'}|r|n^{2S+1}L_J\rangle$ are given in Table II and III and were evaluated using the wave functions given by the relativized quark model [6]. Relativistic corrections are implicitly included in these E1 transitions through Siegert's theorem [44–46], by including spin-dependent interactions in the Hamiltonian used to calculate the meson masses and wave functions. The E1 radiative widths are given in Table II and III and compared to other predictions in Table IV.

Most of the predictions for E1 transitions are in qualitative agreement. While most differences are due to differences in phase space arising from different mass predictions the more interesting differences arise from wave function effects. The largest differences are for decays involving the P_1 and P_1' states which are mixtures of the spin singlet $^1P_1$ and spin triplet $^3P_1$ states. These can be traced back to the different $^3P_1 - ^1P_1$mixing angles predicted by the different models. Wave function effects also appear in decays from radially excited states to ground state mesons such as $2^3P_0 \rightarrow 1^3S_1\gamma$ which varies from one to 22 keV. Because the 2^3P_0 has a node in its wave function there will be a cancellation between different pieces of the $\langle 2^3P_0|r|^3S_1\rangle$ overlap integral. Ebert, Faustov, and Galkin [12] include an additional relativistic correction to transitions involving the mixed states caused by the difference of the c and b quark masses. This leads to further differences with the other models.

Radiative transitions which flip spin are described by magnetic dipole (M1) transitions. The rates for magnetic

TABLE II. E1 transition rates. The matrix elements were obtained using the wave functions of the GI model [6]. For mixed states such as $^1P_1'$ and $^1P_1$ the widths are calculated using the wave function conventions defined in Eq. (11) with the mixing angles given in Table I and the matrix elements and C_{fi} factors corresponding to the labelling of column 6.

Initial state	Final state	M_i(MeV)	M_f(MeV)	ω(MeV)	$i \to f$	$\langle f\|r\|i\rangle$(GeV^{-1})	C_{fi}	Width (keV)
1^3P_2	$1^3S_1\gamma$	6768	6338	416	$1^3P_2 \to 1^3S_1$	1.421	$\frac{1}{3}$	83
$1P_1'$	$1^3S_1\gamma$	6750	6338	399	$1^3P_1 \to 1^3S_1$	1.435	$\frac{1}{3}$	11
	$1^1S_0\gamma$		6271	462	$1^1P_1 \to 1^1S_0$	1.288	$\frac{1}{3}$	80
$1P_1$	$1^3S_1\gamma$	6741	6338	391	$1^3P_2 \to 1^3S_1$	1.435	$\frac{1}{3}$	60
	$1^1S_0\gamma$		6271	454	$1^1P_1 \to 1^1S_0$	1.288	$\frac{1}{3}$	13
1^3P_0	$1^3S_1\gamma$	6706	6338	358	$1^3P_0 \to 1^3S_1$	1.443	$\frac{1}{3}$	55
2^3S_1	$1^3P_2\gamma$	6887	6768	118	$2^3S_1 \to 1^3P_2$	-1.914	$\frac{5}{9}$	5.7
	$1P_1'\gamma$		6750	136	$2^3S_1 \to 1^3P_1$	-1.777	$\frac{1}{3}$	0.7
	$1P_1\gamma$		6741	144	$2^3S_1 \to 1^3P_1$	-1.777	$\frac{1}{3}$	4.7
	$1^3P_0\gamma$		6706	179	$2^3S_1 \to 1^3P_0$	-1.620	$\frac{1}{9}$	2.9
2^1S_0	$1P_1'\gamma$	6855	6750	104	$2^1S_0 \to 1^1P_1$	-1.909	1	6.1
	$1P_1\gamma$		6741	113	$2^1S_0 \to 1^1P_1$	-1.909	1	1.3
1^3D_3	$1^3P_2\gamma$	7045	6768	272	$1^3D_3 \to 1^3P_2$	2.383	$\frac{2}{5}$	78
$1D_2'$	$1^3P_2\gamma$	7036	6768	263	$1^3D_2 \to 1^3P_2$	2.389	$\frac{1}{10}$	8.8
	$1P_1'\gamma$		6750	280	$1^1D_2 \to 1^1P_1$	2.306	$\frac{2}{5}$	63
	$1P_1\gamma$		6741	289	$1^1D_2 \to 1^1P_1$	2.306	$\frac{2}{5}$	7.0
$1D_2$	$1^3P_2\gamma$	7041	6768	268	$1^3D_2 \to 1^3P_2$	2.389	$\frac{1}{10}$	9.6
	$1P_1'\gamma$		6750	285	$1^3D_2 \to 1^3P_1$	2.274	$\frac{3}{10}$	15
	$1P_1\gamma$		6741	294	$1^3D_2 \to 1^3P_1$	2.274	$\frac{3}{10}$	64
1^3D_1	$1^3P_2\gamma$	7028	6768	255	$1^3D_1 \to 1^3P_2$	2.391	$\frac{1}{90}$	1.8
	$1P_1'\gamma$		6750	273	$1^3D_1 \to 1^3P_1$	2.281	$\frac{1}{6}$	4.4
	$1P_1\gamma$		6741	281	$1^3D_1 \to 1^3P_1$	2.281	$\frac{1}{6}$	28
	$1^3P_0\gamma$		6706	315	$1^3D_1 \to 1^3P_0$	2.152	$\frac{2}{9}$	55
2^3P_2	$2^3S_1\gamma$	7164	6887	272	$2^3P_2 \to 2^3S_1$	2.195	$\frac{1}{3}$	55
	$1^3S_1\gamma$		6338	778	$2^3P_2 \to 1^3S_1$	0.2308	$\frac{1}{3}$	14
	$1^3D_3\gamma$		7045	118	$2^3P_2 \to 1^3D_3$	-2.072	$\frac{14}{25}$	6.8
	$1D_2'\gamma$		7036	127	$2^3P_2 \to 1^3D_2$	-1.970	$\frac{1}{10}$	0.7
	$1D_2\gamma$		7041	122	$2^3P_2 \to 1^3D_2$	-1.970	$\frac{1}{10}$	0.6
	$1^3D_1\gamma$		7028	135	$2^3P_2 \to 1^3D_1$	-1.866	$\frac{1}{150}$	0.1
$2P_1'$	$2^3S_1\gamma$	7150	6887	258	$2^3P_1 \to 2^3S_1$	2.319	$\frac{1}{3}$	5.5
	$2^1S_0\gamma$		6855	289	$2^1P_1 \to 2^1S_0$	2.046	$\frac{1}{3}$	52
	$1^3S_1\gamma$		6338	769	$2^3P_1 \to 1^3S_1$	0.155	$\frac{1}{3}$	0.6
	$1^1S_0\gamma$		6271	825	$2^1P_1 \to 1^1S_0$	0.254	$\frac{1}{3}$	19
	$1D_2'\gamma$		7036	113	$2^3P_1 \to 1^3D_2$	-2.096	$\frac{1}{2}$	5.5
	$1D_2\gamma$		7041	108	$2^1P_1 \to 1^1D_2$	-2.080	$\frac{2}{3}$	1.3
	$1^3D_1\gamma$		7028	121	$2^3P_1 \to 1^3D_1$	-1.996	$\frac{1}{6}$	0.2
$2P_1$	$2^3S_1\gamma$	7145	6887	253	$2^3P_1 \to 2^3S_1$	2.319	$\frac{1}{3}$	45
	$2^1S_0\gamma$		6855	284	$2^1P_1 \to 2^1S_0$	2.046	$\frac{1}{3}$	5.7
	$1^3S_1\gamma$		6338	761	$2^3P_1 \to 1^3S_1$	0.155	$\frac{1}{3}$	5.4
	$1^1S_0\gamma$		6271	820	$2^1P_1 \to 1^1S_0$	0.254	$\frac{1}{3}$	2.1
	$1D_2'\gamma$		7036	108	$2^3P_1 \to 1^3D_2$	-2.096	$\frac{1}{2}$	0.8
	$1D_2\gamma$		7041	103	$2^1P_1 \to 1^1D_2$	-2.080	$\frac{2}{3}$	3.6
	$1^3D_1\gamma$		7028	116	$2^3P_1 \to 1^3D_1$	-1.996	$\frac{1}{6}$	1.6
2^3P_0	$2^3S_1\gamma$	7122	6887	231	$2^3P_0 \to 2^3S_1$	2.437	$\frac{1}{3}$	42
	$1^3S_1\gamma$		6338	741	$2^3P_0 \to 1^3S_1$	0.066	$\frac{1}{3}$	1.0
	$1^3D_1\gamma$		7028	93	$2^3P_0 \to 1^3D_1$	-2.128	$\frac{2}{3}$	4.2

TABLE III. E1 transition rates (continued).

Initial state	Final state	M_i (MeV)	M_f(MeV)	ω(MeV)	$i \to f$	$\langle f\|r\|i\rangle$GeV^{-1})	C_{fi}	Width (keV)
1^3F_4	$1^3D_3\gamma$	7271	7045	222	$1^3F_4 \to 1^3D_3$	3.156	$\frac{3}{7}$	81
$1F_3'$	$1^3D_3\gamma$	7266	7045	218	$1^3F_3 \to 1^3D_3$	3.159	$\frac{1}{21}$	3.7
	$1D_2'\gamma$		7036	226	$1^1F_3 \to 1^1D_2$	3.104	$\frac{3}{7}$	78
	$1D_2\gamma$		7041	222	$1^3F_3 \to 1^3D_2$	3.091	$\frac{8}{21}$	0.5
$1F_3$	$1^3D_3\gamma$	7276	7045	227	$1^3F_3 \to 1^3D_3$	3.159	$\frac{1}{21}$	5.4
	$1D_2'\gamma$		7036	236	$1^1F_3 \to 1^1D_2$	3.104	$\frac{3}{7}$	0.04
	$1D_2\gamma$		7041	231	$1^3F_3 \to 1^3D_2$	3.091	$\frac{8}{21}$	82
1^3F_2	$1^3D_3\gamma$	7269	7045	221	$1^3F_2 \to 1^3D_3$	3.160	$\frac{1}{525}$	0.4
	$1D_2'\gamma$		7041	224	$1^3F_2 \to 1^3D_2$	3.095	$\frac{1}{15}$	6.3
	$1D_2\gamma$		7036	229	$1^3F_2 \to 1^3D_2$	3.095	$\frac{1}{15}$	6.5
	$1^3D_1\gamma$		7028	237	$1^3F_2 \to 1^3D_1$	3.026	$\frac{9}{25}$	75

dipole transitions in quarkonium bound states are given in the nonrelativistic approximation by [47,48]

$$\Gamma(i \to f\gamma) = \frac{\alpha}{3}\mu^2\omega^3(2J_f + 1)|\langle f|j_0(kr/2)|i\rangle|^2 \quad (15)$$

where

$$\mu = \frac{e_c}{m_c} - \frac{e_{\bar{b}}}{m_{\bar{b}}}, \quad (16)$$

e_c and $e_{\bar{b}}$ are the c-quark and b-antiquark charges in units of $|e|$ ($e_c = 2/3$ and $e_{\bar{b}} = 1/3$), and m_c and m_b are the quark masses given above.

The M1 widths and overlap integrals are given in Table V. They are compared to other calculations in Table VI. Transitions in which the principle quantum number changes are referred to as hindered transitions which are not allowed in the nonrelativistic limit due to the orthogonality of the wave functions. M1 transitions, especially hindered transitions, are notorious for their sensitivity to relativistic corrections [49]. In our calculations the wave function orthogonality is broken by including a smeared hyperfine interaction directly in the Hamiltonian so that the $^3S_1$ and $^1S_0$ states have slightly different wave functions. Ebert *et al.* are more rigorous in how they include relativistic corrections [12] but to improve the $J/\psi \to \eta_c\gamma$ result they modify the confining potential by making it a linear combination of Lorentz vector and Lorentz scalar pieces.

Given the sensitivity of radiative transitions to details of the models, precise measurements of electromagnetic transition rates would provide stringent tests of the various calculations.

IV. HADRONIC TRANSITIONS

Hadronic transitions between quarkonium levels are needed to estimate branching ratios and discuss search strategies for these states. In fact, these are the dominant decays for both the $\psi(2S)$ and $\Upsilon(2S)$ states. There have been numerous theoretical estimates of hadronic transitions over the years [30,31,50–60]. In some cases the estimates disagree by orders of magnitude [52]. Hadronic transitions are typically described as a two-step process in which the gluons are first emitted from the heavy quarks and then recombine into light quarks. A multipole expansion of the color gauge field is employed to describe the emission process where the intermediate color octet quarkonium state is modeled by some sort of quarkonium hybrid wave function. However, the main disagreement between predictions arises from how the rehadronization step is estimated. To some extent this latter uncertainty can be reduced by employing the multipole expansion of the color gauge fields developed by Yan and collaborators [30,31,50,51] together with the Wigner-Eckart theorem to estimate the E1-E1 transition rates [30] and fixing the reduced matrix elements by rescaling measured transition rates. When no measured transitions exist we instead rescale the theoretical estimates of related matrix elements [31]. This is the approach used by Eichten and Quigg [2]. In addition to E1-E1 transitions there will be other transitions such as $^3S_1 \to {}^3S_1 + \eta$ which goes via M1-M1 & E1-M2 multipoles and spin-flip transitions such as $^3S_1 \to {}^1P_1\pi\pi$ which goes via E1-M1 [31]. These transitions are suppressed by inverse powers of the quark masses and are expected to be small compared to the E1-E1 and electromagnetic transitions. The $2^3S_1 \to 1^3S_1 + \eta$ transitions are further suppressed due to being at the limit of available phase space.

The differential rate for E1-E1 transitions from an initial quarkonium state Φ' to the final quarkonium state Φ, and a system of light hadrons, h, is given by the expression [30,31]:

$$\frac{d\Gamma}{d\mathcal{M}^2}[\Phi' \to \Phi + h] = (2J + 1)\sum_{k=0}^{2}\begin{Bmatrix} k & \ell' & \ell \\ s & J & J' \end{Bmatrix}^2 A_k(\ell', \ell) \quad (17)$$

TABLE IV. Comparison of predictions for E1 transition rates. The column labeled GI is the present work. We quote the predicted rates from the various references and do not attempt to normalize the rates to common phase space factors.

Initial state	Final state	Widths (keV)					
		GI [6]	EFG [12]	GKLT [5]	EQ [2]	GJ [9]	FU [10]
1^3P_2	$1^3S_1\gamma$	83	107	102.9	112.6	73.6	126
$1P_1'$	$1^3S_1\gamma$	11	13.6	8.1	0.1	10.5	26.2
	$1^1S_0\gamma$	80	132	131.1	56.4	66.6	128
$1P_1$	$1^3S_1\gamma$	60	78.9	77.8	99.5	49.0	75.8
	$1^1S_0\gamma$	13	18.4	11.6	0.0	16.6	32.5
1^3P_0	$1^3S_1\gamma$	55	67.2	65.3	79.2	43.0	74.2
2^3S_1	$1^3P_2\gamma$	5.7	5.18	14.8	17.7	4.0	14.5
	$1P_1'\gamma$	0.7	0.63	1.0	0.0	0.6	2.5
	$1P_1\gamma$	4.7	5.05	12.8	14.5	3.6	13.3
	$1^3P_0\gamma$	2.9	3.78	7.7	7.8	2.6	9.6
2^1S_0	$1P_1'\gamma$	6.1	3.72	15.9	5.2	3.6	13.1
	$1P_1\gamma$	1.3	1.02	1.9	0.0	1.3	6.4
1^3D_3	$1^3P_2\gamma$	78	102	76.9	98.7		
$1D_2'$	$1^3P_2\gamma$	8.8	12.8	6.8			
	$1P_1'\gamma$	63	116	46.0	92.5[a]		
	$1P_1\gamma$	7.0	7.25	25.0			
$1D_2$	$1^3P_2\gamma$	9.6	27.5	12.2	24.7[a]		
	$1P_1'\gamma$	15	14.1	18.4	0.1[a]		
	$1P_1\gamma$	64	112	44.6	88.8[a]		
1^3D_1	$1^3P_2\gamma$	1.8	5.52	2.2	2.7		
	$1P_1'\gamma$	4.4	7.66	3.3	0.0		
	$1P_1\gamma$	28	73.8	39.2	49.3		
	$1^3P_0\gamma$	55	128	79.7	88.6		
2^3P_2	$2^3S_1\gamma$	55	57.3	49.4	73.8		
	$1^3S_1\gamma$	14		19.2	25.8		
	$1^3D_3\gamma$	6.8	1.59	10.9	17.8		
	$1D_2'\gamma$	0.7	0.113	0.5			
	$1D_2\gamma$	0.6	0.269	1.5	3.2[a]		
	$1^3D_1\gamma$	0.1	0.035	0.1	0.2		
$2P_1'$	$2^3S_1\gamma$	5.5	9.1	5.9	5.4		
	$2^1S_0\gamma$	52	72.5	58.0			
	$1^3S_1\gamma$	0.6		2.5	2.1		
	$1^1S_0\gamma$	19		20.1			
	$1D_2'\gamma$	5.5	1.2	3.5			
	$1D_2\gamma$	1.3	0.149	2.5	11.5[a]		
	$1^3D_1\gamma$	0.2	0.073	0.3	0.4		
$2P_1$	$2^3S_1\gamma$	45	37.9	32.1	54.3		
	$2^1S_0\gamma$	5.7	11.7	8.1			
	$1^3S_1\gamma$	5.4		15.3	22.1		
	$1^1S_0\gamma$	2.1		3.1			
	$1D_2'\gamma$	0.8	0.021	1.2			
	$1D_2\gamma$	3.6	0.418	3.9	9.8[a]		
	$1^3D_1\gamma$	1.6	0.184	1.6	0.3		
2^3P_0	$2^3S_1\gamma$	42	29.2	25.5	41.2		
	$1^3S_1\gamma$	1.0		16.1	21.9		
	$1^3D_1\gamma$	4.2	0.036	3.2	6.9		

[a]We identify the $1D_2'$ and $1D_2$ states with the $^1D_2$ and $^3D_2$ states of Eichten and Quigg [2]

where ℓ', ℓ are the orbital angular momentum and J', J are the total angular momentum of the initial and final states, respectively, s is the spin of the $Q\bar{Q}$ pair, $\mathcal{M}^2$ is the invariant mass squared of the light hadron system, $\{\cdots\}$ is a $6-j$ symbol, and $A_k(\ell',\ell)$ are the reduced matrix elements. The magnitudes of the $A_k(\ell',\ell)$ are model dependent with a large variation in their estimates. In the soft-pion limit the A_1 contributions are suppressed so, as

TABLE V. M1 transition rates. The matrix elements were obtained using the wave functions of the GI model [6].

Initial state	Final state	M_i(MeV)	M_f(MeV)	ω(MeV)	$\langle f\|j_0(kr/2)\|i\rangle$(GeV^{-1})	Width (keV)
1^3S_1	$1^1S_0\gamma$	6338	6271	67	0.995	0.08
2^3S_1	$2^1S_0\gamma$	6887	6855	32	0.992	0.01
	$1^1S_0\gamma$		6271	588	0.102	0.6
2^1S_0	$1^3S_1\gamma$	6855	6338	498	-0.57	0.3
3^3S_1	$3^1S_0\gamma$	7272	7250	22	0.992	0.003
	$2^1S_0\gamma$		6855	405	0.109	0.2
	$1^1S_0\gamma$		6271	932	0.05	0.6
3^1S_0	$2^3S_1\gamma$	7250	6887	354	-0.04	0.06
	$1^3S_1\gamma$		6338	855	0.09	4.2

is the usual practice, we will take $A_1(\ell', \ell) = 0$. For the remaining rates we use scaling arguments taking measured rates as input or, when no measured rates exist, we rescale the rates predicted for the $b\bar{b}$ system by Kuang and Yan [31] to obtain the $c\bar{b}$ rates. The amplitudes for E1-E1 transitions depend quadratically on the interquark separation so the scaling law between a $c\bar{b}$ rate and the corresponding $Q\bar{Q}$ rate is given by [30]

$$\frac{\Gamma(c\bar{b})}{\Gamma(Q\bar{Q})} = \frac{\langle r^2(c\bar{b})\rangle^2}{\langle r^2(Q\bar{Q})\rangle^2} \tag{18}$$

up to phase space. The scaling factors used to relate the input rates to the $c\bar{b}$ rates are given in Table VII.

There is a large variation in the reduced rates. For example, for the transition $1^3D_1 \to 1^3S_1 + \pi\pi$ estimates for $A_2(2, 0)$ differ by almost 3 orders of magnitude [31,52,59,60]. We point this out as a cautionary note to the reader. The reduced rates are summarized in Table VII. For the $2^3S_1 \to 1^3S_1 + \pi\pi$ reduced rate we take an average of the results taken from rescaling the $\psi' \to J/\psi + \pi\pi$ and $\Upsilon(2S) \to \Upsilon + \pi\pi$ rates. The $3^3S_1 \to 2^3S_1 + \pi\pi$ and $3^3S_1 \to 2^3S_1 + \pi\pi$ values were obtained by rescal-

TABLE VI. Comparison of M1 partial widths. All widths are given in eV. Note that no effort has been made to scale the results to a common phase space.

Initial state	Final state	GI	EFG [12]	GKLT [5]	EQ [2]	FU [10]
1^3S_1	$1^1S_0\gamma$	80	33	60	134.5	59
2^3S_1	$2^1S_0\gamma$	10	17	10	28.9	12
	$1^1S_0\gamma$	600	428	98	123.4	122
2^1S_0	$1^3S_1\gamma$	300	488	96	93.3	139

TABLE VII. Estimates of reduced rates for E1-E1 hadronic transitions between $c\bar{b}$ levels.

Transition	$(Q\bar{Q})$: rate (keV)	$\langle r^2(c\bar{b})\rangle/\langle r^2(Q\bar{Q})\rangle$	Reduced $c\bar{b}$ rate (keV)
$2^3S_1 \to 1^3S_1 + \pi\pi$	$(c\bar{c})$: 146 ± 14 [a]	0.75	$A_0(0, 0) = 82 \pm 8$
	$(b\bar{b})$: 12.2 ± 2 [a]	1.63	$A_0(0, 0) = 33 \pm 5$
	Average		57 ± 7
$3^3S_1 \to 2^3S_1 + \pi\pi$	$(b\bar{b})$: 1.26 ± 0.25 [a]	1.56	$A_0'(0, 0) = 3.1 \pm 0.6$
$3^3S_1 \to 1^3S_1 + \pi\pi$	$(b\bar{b})$: 1.72 ± 0.25 [a]	1.56	$A_0''(0, 0) = 4.2 \pm 0.6$
$2^3P_0 \to 1^3P_0 + \pi\pi$	$(b\bar{b})$: 0.4 [b]	1.56	$A_0(1, 1) = 2.92$
$2^3P_2 \to 1^3P_1 + \pi\pi$	$(b\bar{b})$: 0.01 [b]	1.57	$A_2(1, 1) = 0.164$
$1^3D_1 \to 1^3S_1 + \pi\pi$	$(c\bar{c})$: 120 ± 57 [c]	0.78	$A_2(2, 0) = 360 \pm 170$
	$(c\bar{c})$: <92 90% C.L. [d]	0.78	$A_2(2, 0) < 280$
	$(b\bar{b})$: 24 [e]	1.6	$A_2(2, 0) = 307$
	$(b\bar{b})$: 0.07 [f]	1.6	$A_2(2, 0) = 0.9$
	$(b\bar{b})$: 0.56 ± 0.07 [g]	1.6	$A_2(2, 0) = 7.2$

[a]From PDG Ref.[61]
[b]From Kuang and Yan using model C: modified Richardson potential Ref. [31]
[c]From BES Ref.[62]
[d]CLEO 90% C.L. upper limit [63]
[e]From Kuang and Yan using model A: linear plus Coulomb potential Ref. [31]
[f]From Moxhay Ref. [59]
[g]From BR prediction of Ko [60]

ing the corresponding $b\bar{b}$ transitions [61]. $A_0(1,1)$ and $A_2(1,1)$, corresponding to $2^3P_0 \to 1^3P_0 + \pi\pi$ and $2^3P_2 \to 1^3P_1 + \pi\pi$ respectively, were obtained by rescaling the appropriate $b\bar{b}$ rate predictions given by Kuang and Yan [31]. As pointed out above there is considerable variation in the $A_2(2,0)$ amplitude needed for the $1^3D_J \to 1^3S_1 + \pi\pi$ transitions. The largest predicted rate for the $\Upsilon(1D) \to \Upsilon(1S) + \pi\pi$ transition comes from Kuang and Yan [31] and has been ruled out by a recent CLEO limit [64]. The CLEO limit is about a factor of 3 larger than the rate predicted by Ko [60]. The reduced rate for the $c\bar{b}$ system found by rescaling the recent BES measurement [62] of the $\psi'' \to J/\psi\pi\pi$ rate is considerably larger than the rate found by rescaling the $\Upsilon(1D) \to \Upsilon(1S) + \pi\pi$ CLEO limit. However, it is likely that one can reconcile the $b\bar{b}$ and $c\bar{c}$ results by properly taking into account $2^3S_1 - 1^3D_1$ mixing [51,65,66]. We will therefore assume a reduced rate of $A_2(2,0) = 21$ keV which is based on the CLEO limit on the transition $\Upsilon(1D) \to \Upsilon(1S) + \pi\pi$ [64]. The $1D \to 1S\pi\pi$ transitions is the subject of recent interest [52,65,66] and as the experimental measurements improve it would be useful to revisit these calculations. The uncertainty in these hadronic transitions could easily lead to factors of two errors in the resulting branching ratios. A final note is that we have not considered coupled channel effects to $D\bar{D}$ and $B\bar{B}$ for the $c\bar{c}$ and $b\bar{b}$ states, respectively, which could make a considerable contribution to states close to threshold [66].

The reduced rates of Table VII are used to obtain the $c\bar{b}$ hadronic transitions which are summarized in Table VIII. We do not include decays of the type $2^{3,1}P_J \to 1^{3,1}P_{J'}$, as they are expected to be small compared to the decays we included. Likewise, transitions with η and π^0 in the final state are possible but are expected to have much smaller partial widths and η transitions are further suppressed by phase space. Although the 3^3S_1 and 3^1S_0 states are expected to be above BD threshold, and therefore relatively broad, we include the two-pion transitions for the sake of completeness.

V. WEAK DECAYS

The final ingredient needed in a study of B_c phenomenology is the B_c width and its weak decay partial widths. The details of B_c decay have been given elsewhere [67–76]. For completeness we give a brief overview of the essential features of these decays and summarize the weak decay branching ratios in Table X. We refer the interested reader to the original literature for details of the calculations [32,67–76].

For a rough estimate of the B_c width we can treat the $\bar{b}$-quark and c-quark decay independently so that B_c decay can be divided into three classes: (i) the $\bar{b}$-quark decay with spectator c-quark, (ii) the c-quark decay with spectator $\bar{b}$-quark, and (iii) the annihilation $B_c^+ \to \ell^+\nu_\ell(c\bar{s}, u\bar{s})$, where $\ell = e, \mu, \tau$. The total width is the sum over partial widths

$$\Gamma(B_c \to X) = \Gamma(b \to X) + \Gamma(c \to X) + \Gamma(ann) \quad (19)$$

In addition there is a Pauli interference contribution to the $\bar{b} \to \bar{c}c\bar{s}$ decay from the c-quark spectator which we ignore in this crude estimate.

In the spectator approximation:

$$\Gamma(\bar{b} \to X) = \frac{9G_F^2|V_{cb}|^2 m_b^5}{192\pi^3} \simeq 4.8 \times 10^{-4}\ \text{eV} \quad (20)$$

and

$$\Gamma(c \to X) = \frac{5G_F^2|V_{cs}|^2 m_c^5}{192\pi^3} \simeq 3.3 \times 10^{-4}\ \text{eV} \quad (21)$$

where we used $|V_{cb}| = 0.0412$, $|V_{cs}| = 0.974$, $m_b = 4.25$ GeV, and $m_c = 1.25$ GeV [61].

Annihilation widths such as $c\bar{b} \to \ell\nu_\ell$ are given by the expression

$$\Gamma = \frac{G_F^2}{8\pi}|V_{bc}|^2 f_{B_c}^2 M_{B_c} \sum_i m_i^2 \left(1 - \frac{m_i^2}{M_{B_c}^2}\right)^2 C_i \quad (22)$$

where m_i is the mass of the heavier fermion in the given decay channel. For lepton channels $C_i = 1$ while for quark channels $C_i = 3|V_{qq'}|^2$. The pseudoscalar decay constant, f_{B_c}, is defined by:

$$\langle 0|\bar{b}(x)\gamma^\mu\gamma_5 c(x)|B_c(k)\rangle = i f_{B_c} V_{cb} k^\mu \quad (23)$$

where V_{cb} is the cb element of the Cabibbo-Kobayashi-Maskawa matrix, and k^μ is the four-momentum of the B_c meson. In the nonrelativistic limit the pseudoscalar decay constant is proportional to the wave function at the origin and is given by the van Royen-Weisskopf formula

$$f_{B_c} = \frac{2\sqrt{3}}{M}\psi(0). \quad (24)$$

This result is modified by QCD corrections and relativistic effects, which are included using the Mock-Meson approach or other relativistic quark models. The predictions of the various calculations including Lattice QCD are summarized in Table IX. Using the mock-meson result of $f_{B_c} = 410$ MeV [32], which is consistent with most other predictions, leads to the annihilation width of

$$\Gamma(ann) = 67 \times 10^{-6}\ \text{eV} \quad (25)$$

Adding this result to the spectator contributions gives $\Gamma(\text{total}) = 8.8 \times 10^{-4}$ eV corresponding to a B_c lifetime of $\tau = 0.75$ ps which is in rough agreement with the measured value of $\tau = 0.46^{+0.18}_{-0.16}$ ps. A more careful calculation by Kiselev gives $\tau = 0.5$ ps [67]. The approximate branching fractions for the b-decay, c-decay, and annihilation processes are 54%, 38%, and 8% respec-

TABLE VIII. Rates for two-pion E1-E1 hadronic transitions. The reduced rates are denoted by $A_k(\ell', \ell)$ where k is the rank of the irreducible tensor and ℓ' and ℓ are the orbital angular momenta of the initial and final states.

Transition	Expression for Rate	$(c\bar{b})$ rate (keV)
$2^3S_1 \to 1^3S_1 + \pi\pi$	$A_0(0,0)$	57 ± 7
$2^1S_0 \to 1^1S_0 + \pi\pi$	$A_0(0,0)$	57 ± 7
$3^3S_1 \to 2^3S_1 + \pi\pi$	$A_0'(0,0)$	3.1 ± 0.6
$3^1S_0 \to 2^1S_0 + \pi\pi$	$A_0'(0,0)$	3.1 ± 0.6
$3^3S_1 \to 1^3S_1 + \pi\pi$	$A_0''(0,0)$	4.2 ± 0.6
$3^1S_0 \to 1^1S_0 + \pi\pi$	$A_0''(0,0)$	4.2 ± 0.6
$2^3P_2 \to 1^3P_2 + \pi\pi$	$\frac{1}{3}A_0(1,1) + \frac{1}{4}A_1(1,1) + \frac{7}{60}A_2(1,1)$	1.0
$2^3P_2 \to 1P_1' + \pi\pi$	$\frac{1}{12}A_1(1,1) + \frac{3}{20}A_2(1,1)$[a]	0.004[b]
$2^3P_2 \to 1P_1 + \pi\pi$	$\frac{1}{12}A_1(1,1) + \frac{3}{20}A_2(1,1)$[a]	0.021[b]
$2^3P_2 \to 1^3P_0 + \pi\pi$	$\frac{1}{15}A_2(1,1)$	0.011
$2P_1' \to 1^3P_2 + \pi\pi$	$\frac{5}{36}A_1(1,1) + \frac{1}{4}A_2(1,1)$ [c]	0.004[b]
$2P_1 \to 1^3P_2 + \pi\pi$	$\frac{5}{36}A_1(1,1) + \frac{1}{4}A_2(1,1)$[c]	0.037[b]
$2P_1' \to 1P_1' + \pi\pi$	$A_0(1,1) + A_1(1,1) + \frac{1}{3}A_2(1,1)$[d]	1.2[e]
$2P_1' \to 1P_1 + \pi\pi$	$A_0(1,1) + A_1(1,1) + \frac{1}{3}A_2(1,1)$[d]	0.1[e]
$2P_1 \to 1P_1' + \pi\pi$	$\frac{1}{3}A_0(1,1) + \frac{1}{12}A_1(1,1) + \frac{1}{12}A_2(1,1)$[f]	0.02 [e]
$2P_1 \to 1P_1 + \pi\pi$	$\frac{1}{3}A_0(1,1) + \frac{1}{12}A_1(1,1) + \frac{1}{12}A_2(1,1)$[f]	2.7[e]
$2P_1' \to 1^3P_0 + \pi\pi$	$\frac{1}{9}A_1(1,1)$[g]	0
$2P_1 \to 1^3P_0 + \pi\pi$	$\frac{1}{9}A_1(1,1)$[g]	0
$2^3P_0 \to 1^3P_2 + \pi\pi$	$\frac{1}{3}A_2(1,1)$	0.0547
$2^3P_0 \to 1P_1' + \pi\pi$	$\frac{1}{3}A_1(1,1)$[h]	0
$2^3P_0 \to 1P_1 + \pi\pi$	$\frac{1}{3}A_1(1,1)$[h]	0
$2^3P_0 \to 1^3P_0 + \pi\pi$	$\frac{1}{3}A_0(1,1)$	0.97
$1^3D_{1,3} \to 1^3S_1 + \pi\pi$	$\frac{1}{5}A_2(2,0)$[i]	4.3
$1D_2' \to 1^3S_1 + \pi\pi$	$\frac{1}{5}A_2(2,0)$[i]	2.1[b]
$1D_2 \to 1^3S_1 + \pi\pi$	$\frac{1}{5}A_2(2,0)$[i]	2.2[b]
$1D_2' \to 1^1S_0 + \pi\pi$	$\frac{1}{5}A_2(2,0)$[i]	2.2[b]
$1D_2 \to 1^1S_0 + \pi\pi$	$\frac{1}{5}A_2(2,0)$[i]	2.1[b]

[a]The expression is for the $^3P_2 \to {}^3P_1$ transition.
[b]These rates include the appropriate mixing angles defined in Eq. (11) and given in Table I
[c]The expression is for the $^3P_1 \to {}^3P_2$ transition.
[d]The expression is for the $^1P_1 \to {}^1P_1$ transition.
[e]These rates include the appropriate mixing angles. We assume $a + \nu e$ phase between the $^1P_1 \to {}^1P_1$ and $^3P_1 \to {}^3P_1$ amplitudes. The $2P_1' \to 1P_1$ and $2P_1 \to 1P_1'$ widths are most sensitive to this phase. In any case the widths are expected to be quite small and not particularly important.
[f]The expression is for the $^3P_1 \to {}^3P_1$ transition.
[g]The expression is for the $^3P_1 \to {}^3P_0$ transition.
[h]The expression is for the $^3P_0 \to {}^3P_1$ transition.
[i]These correspond to the $^3D_J \to {}^3S_1$ or $^1D_2 \to {}^1S_0$ transitions as appropriate.

tively. These BR's are modified by strong interaction effects [4,67,70–72,74] which are included in some recent calculations of BR's. The branching ratios of some prominent decay modes are summarized in Table X. In addition, weak B_c decays to P-wave charmonium states, χ_c or h_c, are potentially important decay modes [74] but we will neglect them in favor of simpler to observe decay chains.

TABLE IX. Comparison of predictions for the pseudoscalar decay constant of the B_c meson.

GI [32]	EFG [12]	GKLT [5]	EQ [2]	Fu [10]	Ki[68]	Lattice [42]	Lattice [69]
410 ± 40	433	500 ± 80	500 [a]	517	395 ± 15	440 ± 20	420 ± 13

[a]Using Buchmüller-Tye potential.

TABLE X. Branching ratios in % for some prominent exclusive B_c^+ decays.

	Mode	Kis [67]	IKS [70]	CC [a][71]	EFG [73]	NW [72]
B_c^+	$\to J/\psi e^+\nu$	1.9	2.3	2.4	1.2	1.5
	$\to \eta_c e^+\nu$	0.75	0.98	1.0	0.42	0.52
	$\to B^0 e^+\nu$	0.34	0.15	0.16	0.042	0.05
	$\to B^{*0} e^+\nu$	0.58	0.16	0.23	0.12	0.05
	$\to B_s^0 e^+\nu$	4.03	2.0	1.9	0.84	0.94
	$\to B_s^{*0} e^+\nu$	5.06	2.6	3.1	1.75	1.44
	$\to J/\psi\pi^+$	0.13		0.22	0.061	
	$\to J/\psi\rho^+$	0.40		0.66	0.16	
	$\to \eta_c\pi^+$	0.20		0.23	0.085	
	$\to \eta_c\rho^+$	0.42		0.61	0.21	
	$\to B_s^0\pi^+$	16.4		5.1	2.52	
	$\to B_s^0\rho^+$	7.2		3.9	1.41	
	$\to B_s^{*0}\pi^+$	6.5		4.5	1.61	
	$\to B_s^{*0}\rho^+$	20.2		13.1	11.1	
	$\to B_s^0 K^+$	1.06		0.37	0.21	
	$\to B_s^{*0} K^+$	0.37		0.26	0.11	
	$\to B^0\pi^+$	1.06		0.29	0.10	
	$\to B^0\rho^+$	0.96		0.52	0.13	
	$\to B^{*0}\pi^+$	0.95		0.25	0.03	
	$\to B^{*0}\rho^+$	2.57		1.0	0.68	
	$\to B^+\bar{K}^0$	1.98		0.30	0.24	
	$\to B^+\bar{K}^{*0}$	0.43		0.21	0.09	
	$\to B^{*+}\bar{K}^0$	1.60		0.23	0.11	
	$\to B^{*+}\bar{K}^{*0}$	1.67		0.44	0.84	
	$\to \tau^+\nu_\tau$	1.6				
	$\to c\bar{s}$	4.9				

[a]Using the PDG [61]

VI. EXPERIMENTAL SIGNATURES AND SEARCH STRATEGIES

B_c mesons offer a rich spectroscopy of narrow states to study; there are two S-wave, two P-wave, and one D-wave B_c multiplets below BD threshold. Because B_c mesons carry flavor they cannot annihilate into gluons and are expected to be quite narrow; <100 keV. In addition, the F-wave states are just above threshold so might also be relatively narrow due to the angular momentum barrier which would suppress the decay [77]. Two ingredients are necessary for the study of B_c spectroscopy; that they be produced in sufficient quantity and that they yield a signal that can be distinguished from background.

B_c production production proceeds via the hard associative production of the two heavy quark pairs $c\bar{c}$ and $b\bar{b}$ which suppresses the B_c yield relative to beauty hadrons by $\mathcal{O}(10^{-3})$ [19]. Because fragmentation dominates at high-p_T it has proven useful to describe B_c meson production by hadronization of individual high-p_T partons using the factorization formalism based on nonrelativistic QCD [15]. This approach was utilized by a number of authors to calculate B_c production at hadron colliders. At the Tevatron, with acceptance cuts of $p_t > 6$ GeV and $|y| < 1$, Cheung estimates that $\mathcal{O}(10^7)$ B_c mesons should be produced for an integrated luminosity of 1 fb^{-1} [20]. At the LHC $\mathcal{O}(10^9)$ B_c mesons are expected to be produced for 100 fb^{-1} with the kinematic cuts of $p_t > 10$ GeV and $|y(B_c)| < 2.5$ [20]. The B_c^* cross sections are expected to be $50 - 100\%$ larger than the B_c cross sections [16,19,20]. The p_T distribution falls rapidly so that the small p_T region is quite important [16] but also making the cross sections sensitive to the exact values of the kinematic cuts [17,18]. With the high luminosity of the LHC one expects a sizable number of P- and D-wave ($c\bar{b}$) states ($\sim 20\%$ and $\sim 2\%$ of the total inclusive B_c cross section, respectively) as well as excited S-wave states to be produced ($2S/1S \sim 0.6$) [20,22,24]. The LHC should therefore produce sufficient B_c mesons to allow the study of the $c\bar{b}$ spectroscopy and decays. We will use these numbers as the starting point to estimate the number of B_c's produced in a particular decay chain.

Regardless of which state is produced, it will eventually cascade decay to the B_c ground state via electromagnetic and hadronic transitions so that the B_c must be observed in order to reconstruct the parent particle for the particular decay chain. Prominent decays of the B_c are given in Table X. B_c decays with a J/ψ in the final state such as $J/\psi + X$ where X can be a π^+, ρ^+, or $\ell^+\nu_\ell$ are especially useful as the $J/\psi \to \ell^+\ell^-$ provides a use-

ful trigger for B_c events. The golden channel to detect B_c is $B_c \to J/\psi\pi(\rho)$ but their BR's are quite small $\mathcal{O}(0.2-0.4\%)$ resulting in a combined BR for $B_c \to J/\psi + \pi^+ \to \ell'^-\ell'^+\pi^+$ of $\sim$0.02%. This would yield about 2000 events for 1 fb^{-1} integrated luminosity at the Tevatron and about 2×10^5 events for 100 fb^{-1} integrated luminosity at the LHC. The decay $B_c^\pm \to J/\psi\ell^\pm\nu_\ell$ with $J/\psi \to e^+e^-$ has a distinctive signature of three charged leptons coming from a common secondary vertex and has a BR of about 2% resulting in a combined BR for $B_c \to J/\psi\ell^+\nu_\ell \to \ell'^-\ell'^+\ell^+\nu_\ell$ ($\ell = e, \mu$) of about 0.2% yielding 2×10^4 events at the Tevatron and 2×10^6 at the LHC. The trade off is that the semileptonic decay mode $B_c \to J/\psi + \ell\nu_\ell$ has a larger branching ratio but also has missing energy while $B_c^\pm \to J/\psi\pi^\pm$ has a smaller BR but has the advantage that the B_c can be fully reconstructed. In these B_c decays the b quark decays to charm. B_c decays in which the c quark decays, such as $B_c^+ \to B_s^0\pi^+$, have much larger BR's and could also prove to be important modes if B_c's can be reconstructed in these channels.

To estimate event rates we also need to include detection efficiencies. Simulations by D0 and CDF [3] find efficiencies for the exclusive decays $B_c \to J/\psi\pi \to \mu^+\mu^-\pi$ and $B_c \to J/\psi\ell\nu_\ell \to \mu^+\mu^-\ell\nu_\ell$ of $\sim$2% and $\sim$4% respectively.

In Table XI and XII we combine the electromagnetic transitions widths with the hadronic transition widths to give total widths and BR's. These are used in Table XIII to give estimates for the number of events expected at the Tevatron and LHC for the more prominent decay chains of B_c excited states. We assume that the ground B_c state is observed in the $B_c \to J/\psi\ell^+\nu_\ell \to \ell'^-\ell'^+\ell^+\nu_\ell$ and $B_c \to J/\psi + \pi^+ \to \ell'^-\ell'^+\pi^+$ decay modes with BR's 2% and 0.2% respectively and detection efficiencies of $\sim$2% and $\sim$4% respectively. We include a factor of 2 to take into account both the e^+e^- and $\mu^+\mu^-$ decay modes of the J/ψ and a factor of 2 to take into account the production of both charge conjugate B_c states. To take into account the relative production rates of different excited states we use the production rates given above of $10^7 B_c$'s at the Tevatron and $10^9 B_c$'s at the LHC with relative numbers of $\times2$ for the B_c^*, 0.2 for the $1P$ states, 0.02 for the $1D$ states, and 0.6 for the $2S$ relative to the $1S$ states. For the $2P$ states we use the same factor of 0.6 for $2P$ relative to $1P$ but this is a rather arbitrary assumption. As noted already, the cross sections are very sensitive to the kinematic cuts so the number of events expected should only be taken as rough estimates.

The signal for excited B_c states is a photon or pions in coincidence with B_c decay. A serious omission from the estimates given in Table XIII is the neglect of tagging efficiencies for the photons and pions in the transitions. The photon ID can be relatively high depending on the kinematics. For the pions, the combinatorial background is large and π/K separation is not so good so one really needs to do studies of specific processes. Thus, understanding photon and pion identification requires a detailed simulation study which is beyond the scope of this paper. However, one might be optimistic, given the

TABLE XI. Partial widths and branching fractions for strong and electromagnetic transitions. Details of the calculations are given in the text.

Initial state	Final state	Width (keV)	B.F. (%)
1^3S_1	1^1S_0	0.08	100
1^3P_2	1^3S_1	83	100
$1P_1'$	1^3S_1	11	12.1
	1^1S_0	80	87.9
	Total	91	100
$1P_1$	1^3S_1	60	82.2
	1^1S_0	13	17.8
	Total	73	100
1^3P_0	1^3S_1	55	100
2^1S_0	$1^1S_0 + \pi\pi$	57 ± 7	88.1
	$1P_1' + \gamma$	6.1	9.4
	$1P_1 + \gamma$	1.3	2.0
	$1^3S_1 + \gamma$	0.3	0.5
	Total	64.7	100
2^3S_1	$1^3S_1 + \pi\pi$	57 ± 7	79.6
	$1^3P_2 + \gamma$	5.7	8.0
	$1P_1' + \gamma$	0.7	1.0
	$1P_1 + \gamma$	4.7	6.6
	$1^3P_0 + \gamma$	2.9	4.0
	$2^1S_0 + \gamma$	0.01	1×10^{-2}
	$1^1S_0 + \gamma$	0.6	0.8
	Total	71.6	100
1^3D_3	$1^3S_1 + \pi\pi$	4.3	5.2
	$1^3P_2 + \gamma$	78	94.8
	Total	82.3	100
$1D_2'$	$1^3S_1 + \pi\pi$	2.1	2.5
	$1^1S_0 + \pi\pi$	2.2	2.6
	$1^3P_2 + \gamma$	8.8	10.6
	$1P_1' + \gamma$	63	75.8
	$1P_1 + \gamma$	7	8.4
	Total	83.1	100
$1D_2$	$1^3S_1 + \pi\pi$	2.2	2.4
	$1^1S_0 + \pi\pi$	2.1	2.3
	$1^3P_2 + \gamma$	9.6	10.3
	$1P_1' + \gamma$	15	16.1
	$1P_1 + \gamma$	64	68.9
	Total	92.9	100
1^3D_1	$1^3S_1 + \pi\pi$	4.3	4.6
	$1^3P_2 + \gamma$	1.8	1.9
	$1P_1' + \gamma$	4.4	4.7
	$1P_1 + \gamma$	28	29.9
	$1^3P_0 + \gamma$	55	58.8
	Total	93.5	100

TABLE XII. Partial widths and branching fractions for strong and electromagnetic transitions (continued).

Initial state	Final state	Width (keV)	B.F. (%)
2^3P_2	$1^3P_2 + \pi\pi$	1.0	1.3
	$2^3S_1 + \gamma$	55	70.3
	$1^3S_1 + \gamma$	14	17.9
	$1^3D_3 + \gamma$	6.8	8.7
	$1D_2' + \gamma$	0.7	0.9
	$1D_2 + \gamma$	0.6	0.8
	$1^3D_1 + \gamma$	0.1	0.1
	Total	78.2	100
$2P_1'$	$1P_1' + \pi\pi$	1.2	1.4
	$2^3S_1 + \gamma$	5.5	6.4
	$2^1S_0 + \gamma$	52	61.0
	$1^3S_1 + \gamma$	0.6	0.7
	$1^1S_0 + \gamma$	19	22.3
	$1D_2' + \gamma$	5.5	6.4
	$1D_2 + \gamma$	1.3	1.5
	$1^3D_1 + \gamma$	0.2	0.2
	Total	85.3	100
$2P_1$	$1P_1 + \pi\pi$	2.7	4.0
	$2^3S_1 + \gamma$	45	67.3
	$2^1S_0 + \gamma$	5.7	8.5
	$1^3S_1 + \gamma$	5.4	8.1
	$1^1S_0 + \gamma$	2.1	3.1
	$1D_2' + \gamma$	0.8	1.2
	$1D_2 + \gamma$	3.6	5.4
	$1^3D_1 + \gamma$	1.6	2.4
	Total	66.9	100
2^3P_0	$1^3P_0 + \pi\pi$	1.0	2.1
	$2^3S_1 + \gamma$	42	87.1
	$1^3S_1 + \gamma$	1.0	2.1
	$1^3D_1 + \gamma$	4.2	8.7
	Total	48.2	100

TABLE XIII. Expected event rates for various decay chains at the Tevatron and the LHC. The B_c is assumed to decay to $B_c \to J/\psi\pi \to \mu^+\mu^-\pi$ and $B_c \to J/\psi\ell\nu_\ell \to \mu^+\mu^-\ell\nu_\ell$ final states. Details of these estimates are described in the text.

Decay Chain	Tevatron	LHC
$1^3S_1 \xrightarrow{\gamma} B_c$	3.4×10^3	3.4×10^5
$2^1S_0 \xrightarrow{\pi\pi} B_c$	1.8×10^3	1.8×10^5
$2^3S_1 \xrightarrow{\pi\pi} 1^3S_1 \xrightarrow{\gamma} B_c$	1.6×10^3	1.6×10^5
$2^3S_1 \xrightarrow{\gamma} B_c$	16	1.6×10^3
$1^3P_2 \xrightarrow{\gamma} 1^3S_1 \xrightarrow{\gamma} B_c$	6.7×10^2	6.7×10^4
$1P_1' \xrightarrow{\gamma} B_c$	5.9×10^2	5.9×10^4
$1P_1 \to \gamma 1^3S_1 \xrightarrow{\gamma} B_c$	5.5×10^2	5.5×10^4
$1P_1 \xrightarrow{\gamma} B_c$	1.2×10^2	1.2×10^4
$1^3P_0 \xrightarrow{\gamma} 1^3S_1 \xrightarrow{\gamma} B_c$	6.7×10^2	6.7×10^4
$1^3D_3 \xrightarrow{\pi\pi} 1^3S_1 \xrightarrow{\gamma} B_c$	3.5	3.5×10^2
$1^3D_3 \xrightarrow{\gamma} 1^3P_2 \xrightarrow{\gamma} 1^3S_1 \xrightarrow{\gamma} B_c$	64	6.4×10^3
$1D_2' \xrightarrow{\pi\pi} 1^1S_0$	1.7	1.7×10^2
$1D_2' \xrightarrow{\gamma} 1P_1' \xrightarrow{\gamma} B_c$	45	4.5×10^3
$1D_2 \xrightarrow{\pi\pi} 1^1S_0$	1.4	1.4×10^2
$1D_2 \xrightarrow{\gamma} 1P_1' \xrightarrow{\gamma} B_c$	9.5	9.5×10^2
$1D_2 \xrightarrow{\gamma} 1P_1 \xrightarrow{\gamma} B_c$	8.2	8.2×10^2
$1^3D_1 \xrightarrow{\pi\pi} 1^3S_1 \xrightarrow{\gamma} B_c$	3.1	3.1×10^2
$1^3D_1 \xrightarrow{\gamma} 1P_1' \xrightarrow{\gamma} B_c$	2.8	2.8×10^2
$1^3D_1 \xrightarrow{\gamma} 1P_1 \xrightarrow{\gamma} B_c$	3.6	3.6×10^2
$2^3P_2 \xrightarrow{\gamma} 2^3S_1 \xrightarrow{\gamma} B_c$	2.3	2.3×10^2
$2^3P_2 \xrightarrow{\gamma} 1^3S_1 \xrightarrow{\gamma} B_c$	72	7.2×10^3
$2P_1' \xrightarrow{\gamma} B_c$	90	9.0×10^3
$2P_1 \xrightarrow{\gamma} B_c$	12	1.2×10^3
$2P_1 \xrightarrow{\gamma} 2^3S_1 \xrightarrow{\gamma} B_c$	2.2	2.2×10^2
$2^3P_0 \xrightarrow{\gamma} 2^3S_1 \xrightarrow{\gamma} B_c$	2.8	2.8×10^2

success of CDF in studying χ_c production [78] and the observation of the $X(3872) \to J/\psi\pi^+\pi^-$ [79] in $\bar{p}p$ collisions at the Tevatron.

Notwithstanding the previous caveat, it should be possible to observe the $1S$, $2S$, and $1P$ states at the Tevatron. It is also possible, although only marginally so, that some of the $1D$ and $2P$ might also be seen. With the higher statistics available at the LHC, all $c\bar{b}$ states below threshold could potentially be observed, although the larger backgrounds will make this quite challenging.

The fact that the B_c is not an eigenstate of charge conjugation helps simplify the search for states such as the $1P_1'$, $1P_1$, $1D_2'$, and $1D_2$. The singlet component of these states allows E1 or hadronic transitions directly to the ground state B_c with large BR's. This should simplify the reconstruction efforts significantly. For example $1P_1'$ production and decay to the B_c with its subsequent decay to $J/\psi\pi$ and $J/\psi\ell\nu_\ell$ should produce $\mathcal{O}(600)$ events in Run II at the Tevatron. Likewise, $2P_1'$ and its subsequent decay should produce $\mathcal{O}(100)$ events. These yields would be enhanced if other B_c decay modes with larger BR's could be utilized. The discovery of the $1P_1'$ would yield important spectroscopic information in addition to being an experimental tour de force. Of course, these BR's are highly sensitive to the $1P_1' - 1P_1$ mixing angle. With enough measurements these details can be constrained and different models can be differentiated. There will also be large number of events for decay chains going via an intermediate B_c^* such as $2^3S_1 \xrightarrow{\pi\pi} 1^3S_1 \xrightarrow{\gamma} B_c$ and $1^3P_2 \xrightarrow{\gamma} 1^3S_1 \xrightarrow{\gamma} B_c$. However, it will be crucial to detect the 67 keV photon in $B_c^* \to B_c + \gamma$ in these cases, a very challenging experimental task.

VII. SUMMARY

The primary purpose of this paper is to calculate B_c masses and radiative transitions in the relativized quark model. For the most part the mass predictions are consistent with other models, within the accuracy of these models. The largest discrepancy in predictions is for the triplet-singlet mixing angles. This has implications for transitions between states so can be tested with appropriate measurements. Combining the BR's we have calcu-

lated with B_c production cross sections from the literature we see that the $1S$, $1P$, and $2S$ states should be produced in sufficient numbers to be observed at the Tevatron. With the higher statistics of the LHC, it should also be possible to observe the $1D$ and $2P$ states. It will be a significant experimental challenge to extract the signals for these states from the large background but their observation would add considerably to our knowledge of quarkonium spectroscopy and discriminate between the various models that exist in the literature.

ACKNOWLEDGMENTS

The author thanks Vaia Papadimitriou and Manuella Vincter for helpful communications. This research was supported in part the Natural Sciences and Engineering Research Council of Canada.

[1] CDF Collaboration, F. Abe *et al.*, Phys. Rev. D **58**, 112004 (1998).
[2] E. J. Eichten and C. Quigg, Phys. Rev. D **49**, 5845 (1994).
[3] K. Anikeev *et al.*, hep-ph/0201071.
[4] S. S. Gershtein, V.V. Kiselev, A. K. Likhoded, and A.V. Tkabladze, Phys. Usp. **38**, 1 (1995).
[5] S. S. Gershtein, V.V. Kiselev, A. K. Likhoded, and A V. Tkabladze, Phys. Rev. D **51**, 3613 (1995).
[6] S. Godfrey and N. Isgur, Phys. Rev. D **32**, 189 (1985).
[7] Y. Q. Chen and Y. P. Kuang, Phys. Rev. D **46**, 1165 (1992); Erratum: Phys. Rev. D **47**, 350 (1993)]; S. M. Ikhdair and R. Sever, Int. J. Mod. Phys. A **19**, 1771 2004; N. Brambilla and A. Vairo, Phys. Rev. D **62**, 094019 (2000); A. A. Penin, A. Pineda, V. A. Smirnov, and M. Steinhauser, hep-ph/0403080.
[8] J. Zeng, J.W. Van Orden, and W. Roberts, Phys. Rev. D **52**, 5229 (1995).
[9] S. N. Gupta and J. M. Johnson, Phys. Rev. D **53**, 312 (1996).
[10] L. P. Fulcher, Phys. Rev. D **60**, 074006 (1999).
[11] I. P. Gouz, V.V. Kiselev, A. K. Likhoded, V. I. Romanovsky, and O. P. Yushchenko, hep-ph/0211432.
[12] D. Ebert, R. N.Faustov and V. O.Galkin, Phys. Rev. D **67**, 014027 (2003).
[13] W. K. Kwong and J. L. Rosner, Phys. Rev. D **44**, 212 (1991).
[14] S. M. Ikhdair and R. Sever, hep-ph/0406005; S. M. Ikhdair and R. Sever, hep-ph/0403280.
[15] E. Braaten, S. Fleming, and T. C. Yuan, Annu. Rev. Nucl. Part. Sci. **46**, 197 (1996).
[16] C. H. Chang, Y. Q. Chen, and R. J. Oakes, Phys. Rev. D **54**, 4344 (1996).
[17] C. H. Chang and X. G. Wu, hep-ph/0309121.
[18] C. H. Chang, Y. Q. Chen, G. P. Han, and H. T. Jiang, Phys. Lett. B **364**, 78 (1995).
[19] K. M. Cheung, Phys. Rev. Lett. **71**, 3413 (1993).
[20] K. M. Cheung and T. C. Yuan, Phys. Rev. D **53**, 1232 (1996).
[21] Y. Q. Chen, Phys. Rev. D **48**, 5181 (1993).
[22] C. H. Chang and Y. Q. Chen, Phys. Rev. D **48**, 4086 (1993).
[23] T. C. Yuan, Phys. Rev. D **50**, 5664 (1994).
[24] K. M. Cheung and T. C. Yuan, Phys. Rev. D **53**, 3591 (1996).
[25] K. Kolodziej, A. Leike, and R. Ruckl, Phys. Lett. B **355**, 337 (1995).
[26] S. Godfrey and N. Isgur, Phys. Rev. D **34**, 899 (1986); S. Godfrey, Phys. Rev. D **31**, 2375 (1985).
[27] S. Godfrey and R. Kokoski, Phys. Rev. D **43**, 1679 (1991); H. G. Blundell, S. Godfrey, and B. Phelps, Phys. Rev. D **53**, 3712 (1996).
[28] S. Capstick and N. Isgur, Phys. Rev. D **34**, 2809 (1986).
[29] S. Capstick, S. Godfrey, N. Isgur, and J. Paton, Phys. Lett. B **175**, 457 (1986).
[30] T. M.Yan, Phys. Rev. D **22**, 1652 (1980).
[31] Y. P.Kuang and T. M.Yan, Phys. Rev. D **24**, 2874 (1981).
[32] S. Capstick and S. Godfrey, Phys. Rev. D **41**, 2856 (1990).
[33] BABAR Collaboration, B. Aubert *et al.*, Phys. Rev. Lett. **90**, 242001 (2003).
[34] CLEO Collaboration, D. Besson *et al.*, Phys. Rev. D **68**, 032002 (2003).
[35] Belle CollaborationP. Krokovny *et al.*, Phys. Rev. Lett. **91**, 262002 (2003).
[36] Belle CollaborationS. K. Choi *et al.*, Phys. Rev. Lett. **91**, 262001 (2003).
[37] E. J. Eichten, K. Lane, and C. Quigg, Phys. Rev. D **69**, 094019 (2004).
[38] The relativistic kinetic energy is actually that of the spinless Salpeter equation.
[39] D. Gromes, Z. Phys. C **26**, 401 (1984); D. Gromes, in *Proceedings of the Yukon Advanced Study Institute, 1984*, edited by N. Isgur, G. Karl, P. J. O'Donnell, (World Scientific, Singapore, 1985) p. 1.
[40] V. B. Berestetskij, E. M. Lifschitz, and L. P. Pitaevskij, *Relativistic Quantum Theory*, (Oxford, New York, 1971) p. 280.
[41] This is discussed more fully in Appendix A of T. Barnes, N. Black, and P. R. Page, Phys. Rev. D **68**, 054014 (2003).
[42] C. T. H. Davies, K. Hornbostel, G. P. Lepage, A. J. Lidsey, J. Shigemitsu, and J. H. Sloan, Phys. Lett. B **382**, 131 (1996).
[43] See for example W. Kwong and J. L.Rosner, Phys. Rev. D **38**, 279 (1988).
[44] A. J.Siegert, Phys. Rev. **52**, 787 (1937).
[45] R. McClary and N. Byers, Phys. Rev. D **28**, 1692 (1983).
[46] P. Moxhay and J. L.Rosner, Phys. Rev. D **28**, 1132 (1983).
[47] J. D. Jackson, in *Proceedings of the Summer Institute on Particle Physics, 1976*, edited by M. C. Zipf, (Stanford Linear Accelerator Center Report SLAC-198), 1977.

[48] V. A. Novikov, L. B. Okun, M. A. Shifman, A. I. Vainshtein, M. B. Voloshin, and V. I. Zakharov, Phys. Rep. **41**, 1 (1978).
[49] Relativistic effects in M1 transitions are discussed in: J. S. Kang and J. Sucher, Phys. Rev. D **18**, 2698 (1978); H. Grotch and K. J. Sebastian, Phys. Rev. D **25**, 2944 (1982); V. Zambetakis and N. Byers, Phys. Rev. D **28**, 2908 (1983); H. Grotch, D. A. Owen and K. J. Sebastian, Phys. Rev. D **30**, 1924 (1984); X. Zhang, K. J. Sebastian, and H. Grotch, Phys. Rev. D **44**, 1606 (1991).
[50] Y. P.Kuang, S. F. Tuan and T. M.Yan, Phys. Rev. D **37**, 1210 (1988).
[51] Y. P. Kuang and T. M.Yan, Phys. Rev. D **41**, 155 (1990).
[52] J. L. Rosner, Phys. Rev. D **67**, 097504 (2003).
[53] M. B. Voloshin and V. I. Zakharov, Phys. Rev. Lett. **45**, 688 (1980).
[54] V. A. Novikov and M. A. Shifman, Z. Phys. C **8**, 43 (1981).
[55] B. L. Ioffe and M. A. Shifman, Phys. Lett. B **95**, 99 (1980).
[56] M. B. Voloshin, Sov. J. Nucl. Phys. **43**, 1011 (1986).
[57] M. B. Voloshin Phys. Lett. B **562**, 68 (2003).
[58] P. Ko, Phys. Rev. D **52**, 1710 (1995).
[59] P. Moxhay, Phys. Rev. D **37**, 2557 (1988).
[60] P. Ko, Phys. Rev. D **47**, 208 (1993).
[61] Particle Data Group, K. Hagiwara *et al.*, Phys. Rev. D **66**, 010001 (2002).
[62] BES CollaborationJ. Z.Bai *et al.*, hep-ex/0307028.
[63] T. Skwarnicki, Int. J. Mod. Phys. A **19**, 1030 (2004).
[64] CLEO Collaboration, G. Bonvicini *et al.*, Phys. Rev. D **70**, 032001 (2004).
[65] K. Y. Liu and K. T. Chao, hep-ph/0405126 [Phys. Rev. D (to be published)].
[66] J. L. Rosner, hep-ph/0405196.
[67] V. V. Kiselev, hep-ph/0308214.
[68] V. V. Kiselev, hep-ph/0304017.
[69] B. D. Jones and R. M. Woloshyn, Phys. Rev. D **60**, 014502 (1999).
[70] M. A. Ivanov, J. G. Korner, and P. Santorelli, Phys. Rev. D **63**, 074010 (2001).
[71] C. H. Chang and Y. Q. Chen, Phys. Rev. D **49**, 3399 (1994).
[72] M. A. Nobes and R. M. Woloshyn, J. Phys. G **26**, 1079 (2000).
[73] D. Ebert, R. N. Faustov and V. O. Galkin, Phys. Rev. D **68**, 094020 (2003); D. Ebert, R. N. Faustov and V. O. GalkinEur. Phys. J. C **32**, 29 (2003).
[74] C. H. Chang, Y. Q. Chen, G. L. Wang, and H. S. Zong, Phys. Rev. D **65**, 014017 (2002).
[75] D. S. Du and Z. Wang, Phys. Rev. D **39**, 1342 (1989).
[76] A. Y. Anisimov, P. Y. Kulikov, I. M. Narodetsky and K. A. Ter-Martirosian, Phys. At. Nucl. **62**, 1739 (1999).
[77] Related widths in the charmonium system are given in T. Barnes and S. Godfrey, Phys. Rev. D **69**, 054008 (2004); T. Barnes, S. Godfrey, and E. Swanson (to be published); See also Ref. [37].
[78] CDF Collaboration, F. Abe *et al.*, Phys. Rev. Lett. **79**, 578 (1997).
[79] CDF II Collaboration, D. Acosta *et al.*, Phys. Rev. Lett. **93**, 072001 2004.